



# Transport properties and pinning analysis for Co-doped $\text{BaFe}_2\text{As}_2$ thin films on metal tapes

Zhongtang Xu<sup>1</sup> , Pusheng Yuan<sup>1,2</sup>, Fan Fan<sup>1,2</sup>, Yimin Chen<sup>3</sup> and Yanwei Ma<sup>1,2</sup> 

<sup>1</sup> Key Laboratory of Applied Superconductivity, Institute of Electrical Engineering, Chinese Academy of Sciences, Beijing 100190, People's Republic of China

<sup>2</sup> University of Chinese Academy of Sciences, Beijing 100049, People's Republic of China

<sup>3</sup> School of Materials Science and Engineering, Northeastern University, Shenyang 110819, People's Republic of China

E-mail: [ywma@mail.iee.ac.cn](mailto:ywma@mail.iee.ac.cn)

Received 5 January 2018, revised 19 February 2018

Accepted for publication 26 February 2018

Published 23 March 2018



## Abstract

We report on the transport properties and pinning analysis of  $\text{BaFe}_{1.84}\text{Co}_{0.16}\text{As}_2$  (Ba122:Co) thin films on metal tapes by pulsed laser deposition. The thin films exhibit a large in-plane misorientation of  $5.6^\circ$ , close to that of the buffer layer  $\text{SrTiO}_3$  ( $5.9^\circ$ ). Activation energy  $U_0(H)$  analysis reveals a power law relationship with field, having three different exponents at different field regions, indicative of variation from single-vortex pinning to a collective flux creep regime. The Ba122:Co coated conductors present  $T_c^{\text{onset}} = 20.2$  K and  $T_c^{\text{zero}} = 19.0$  K along with a self-field  $J_c$  of  $1.14 \text{ MA cm}^{-2}$  and an in-field  $J_c$  as high as  $0.98$  and  $0.86 \text{ MA cm}^{-2}$  up to  $9$  T at  $4.2$  K for both major crystallographic directions of the applied field, promising for high field applications. Pinning force analysis indicates a significant enhancement compared with similar Ba122:Co coated conductors. By using the anisotropic scaling approach, intrinsic pinning associated with coupling between superconducting blocks can be identified as the pinning source in the vicinity of  $H//ab$ , while for  $H//c$  random point defects are likely to play a role but correlated defects start to be active at high temperatures.

Keywords: pulsed laser deposition, coated conductors, iron-based superconductors, thin films

(Some figures may appear in colour only in the online journal)

## Introduction

The dramatic discovery of superconductivity in layered iron-based materials in 2008 [1, 2] has sparked intense interest in achieving high magnetic field applications and in probing superconductivity mechanisms. With extensive investigation, it has been shown that iron-based superconductors (IBSs) present superior properties that are promising for various superconducting applications, such as wires/tapes, because of their relatively high superconducting transition temperatures,  $T_c$ , (maximum:  $\sim 55$  K) [3], high upper critical magnetic fields,  $H_{c2}$ , [4], and low anisotropy factors,  $\gamma$  [5]. To date, the most promising methods for the fabrication of wires/tapes are

the powder in tube (PIT) and the coated conductor (CC) methods. In particular, global industrial scale production of CCs, which is a fantastic achievement in cuprate development, has resulted in CCs over a kilometer long. However, CCs based on IBSs are still in their infancy compared with cuprate CCs. In fact, IBSs possess advantages over cuprate superconductors in terms of CC technology, especially as IBSs ( $\theta_c \sim 9^\circ$ ) have twice the critical grain boundary misorientation angle for  $J_c$  than cuprates ( $\theta_c \sim 4^\circ$ ) [6]. Therefore, using IBSs for CCs could lead to substantial cost reduction in metal-tape fabrication, compared with cuprate superconductors, where a well textured metal template is necessary. For example, self-field  $J_c$  values higher than  $1 \text{ MA cm}^{-2}$  at

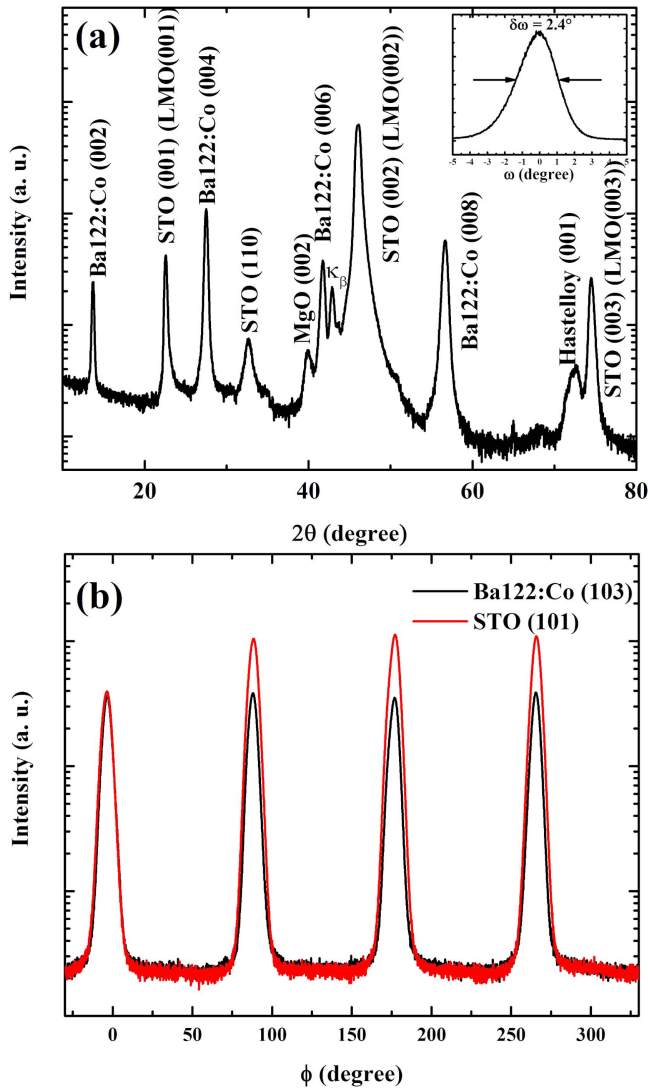


**Figure 1.** (a) Typical out-of-plane XRD patterns of Ba122:Co CCs. The inset shows an out-of-plane rocking curve of the (008) diffraction from the Ba122:Co thin films. (b)  $\phi$  scan of the Ba122:Co (103) and the STO (101) diffractions.

4 K have been realized in  $\text{BaFe}_2(\text{As}_{1-x}\text{P}_x)_2$  (Ba122:P) CCs from poorly aligned metal tapes of  $8^\circ$  [7], which is not suitable for cuprate CCs.

Concerning the current development of IBS CCs, many already developed technologies in cuprate CCs can be used for reference. As in cuprates, two types of metal tapes offering a highly in-plane oriented texture for the growth of thin films have been focused on in IBS CCs: one provides texture by depositing biaxially textured oxide buffer layers on a non-oriented polycrystalline Ni-based Hastelloy flexible metal-tape using the ion beam assisted deposition (IBAD) method. The other uses an oriented Ni–W alloy fabricated by the rolling-assisted biaxially textured substrate (RABiTS) method as the starting metal-tape. IBAD is the most widely used method because the top oxide buffer layers provide a much better texture than that of the RABiTS. Among IBS CCs, the ‘122’ system, such as  $\text{BaFe}_{2-x}\text{Co}_x\text{As}_2$  (Ba122:Co)

and Ba122:P, is most extensively investigated, due to the relatively easy growth of large single crystals and high-quality thin films. For example, Iida *et al* [8] first successfully fabricated a Ba122:Co CC on IBAD-MgO metal tapes with a 10 nm Fe layer to reduce the mismatch between Ba122:Co films and MgO buffer layers. Although the Ba122:Co thin films exhibit good structural properties, their transport properties (self-field  $J_c$  of  $0.1 \text{ MA cm}^{-2}$  at 8 K) are substantially lower than single crystals. With a reduction of the in-plane misorientation of the Ba122:Co thin films down to  $\sim 3^\circ$  and  $1.7^\circ$  [9, 10], great enhancement in the transport properties of Ba122:Co CCs was achieved on IBAD-MgO metal tapes, up to a self-field of  $3.5 \text{ MA cm}^{-2}$  at 2 K, comparable to thin films on single crystal substrates [11]. However, the high field performance ( $\sim 0.1 \text{ MA cm}^{-2}$  at 4 K and 9 T) remains low. Compared with Ba122:Co CCs, Ba122:P CCs exhibit the opposite behavior with in-plane misorientation, in which larger misorientation ( $\sim 8^\circ$ ) leads to higher  $J_c$  because of high-density grain boundaries [7]. In addition, Ba122:P CCs still show exceptional performance above 15 T, comparable to  $\text{Nb}_3\text{Sn}$  [12].

Currently, CCs are extremely promising for realizing IBS applications, but the high field performance requires further enhancement and the pinning mechanism needs to be clarified. In this study, the field and angular dependence of  $J_c$  of Co-doped Ba122 on metal tapes are investigated at various temperatures and fields, showing potential for application, and the pinning mechanism is discussed.

## Experimental details

Ba122:Co films were grown on IBAD- $\text{LaMnO}_3$  (LMO) metal tapes by pulsed laser deposition (PLD) using a KrF excimer laser (wavelength: 248 nm) with a 150 nm  $\text{SrTiO}_3$  (STO) layer between Ba122:Co and LMO. Hastelloy C-276 substrates, 65  $\mu\text{m}$  in thickness and 12 mm in width with a multilayer oxide buffer architecture were used. The fabrication details of the buffer architecture, Hastelloy substrate/ $\text{Al}_2\text{O}_3$ (80 nm)/ $\text{Y}_2\text{O}_3$ (7 nm)/IBAD-MgO(10 nm)/MgO(30 nm)/LMO(100 nm), are described in [13]. The target of nominal composition  $\text{BaFe}_{1.84}\text{Co}_{0.16}\text{As}_2$  with a critical temperature of  $T_c^{\text{zero}} = 24.8 \text{ K}$  was prepared by the solid-state reaction method [11]. STO layers and Ba122:Co thin films were successively deposited at  $850^\circ\text{C}$  in a vacuum of about  $10^{-7}$  Torr; the laser energy density was set to be  $1.4 \text{ J cm}^{-2}$  with a repetition of 9 Hz; the target distance was 40 mm; the films were cooled down to room temperature at a rate of  $10^\circ\text{C min}^{-1}$  after deposition; the thickness of the STO layers (150 nm) and Ba122:Co thin films (110 nm) was controlled by deposition time. Crystal structure and phase purity were measured by x-ray diffraction (XRD) with a  $\text{Cu K}\alpha$  radiation on a Bruker D8 Advance. The transport critical current ( $I_c$ ) at different temperatures and the temperature dependence of resistivity of the films were measured using a standard four-probe configuration by a physical property measurement system (Quantum Design) equipped with a sample rotator. Before the measurement of the transport critical current, micro bridges of 20  $\mu\text{m}$  in width and 100  $\mu\text{m}$  in length were fabricated by conventional

photolithography and Ar<sup>+</sup> etching to reduce the heating effect.  $J_c$ s were calculated from current–voltage ( $I$ – $V$ ) curves with a criterion of  $1 \mu\text{V cm}^{-1}$ .

## Results and discussion

To investigate the phase purity and epitaxial in-plane relationship of the Ba122:Co thin films, we first perform the XRD measurements, as shown in figure 1. Highly  $c$ -axis oriented growth of Ba122:Co thin films can be confirmed from the  $\theta/2\theta$  pattern in figure 1(a), indicative of high phase purity. The full width at half-maximum value of the (008) reflection rocking curve of Ba122:Co thin films is  $\Delta\omega = 2.4^\circ$ , which is larger than the similar thin films deposited on IBAD-MgO metal tapes ( $\Delta\omega = 1.5^\circ$ ) [9] and larger than the Ba122:P thin films on IBAD-MgO metal tapes ( $\Delta\omega = 1.3^\circ$ ) [7]. Furthermore, the in-plane orientation was determined by the  $\varphi$  scans of the off-axis (103) diffraction of Ba122:Co thin films and the (101) diffraction of STO layers, as shown in figure 1(b). The Ba122:Co thin films exhibit a four-fold symmetric peak without extra satellites or additional reflections, due to the tetragonal symmetry. It is thus inferred that the Ba122:Co thin films epitaxially grow on the metal tapes having the orientation relationship of (001)[100] Ba122:Co/(001)[100] STO. The in-plane misorientation of the Ba122:Co thin films and STO layers is  $\Delta\varphi \sim 5.6^\circ$  and  $5.9^\circ$ , respectively, indicating that the texture of the STO layers determines that of the Ba122:Co thin films. Such behavior is different from that of the Ba122:Co thin films on IBAD-MgO metal tapes, in which  $\Delta\varphi_{\text{Ba122:Co}} = 3.2\text{--}3.5^\circ$  regardless of the larger  $\Delta\varphi_{\text{MgO}} = 5.5\text{--}7.3^\circ$  of the MgO buffer layers [9]. The above difference may be caused by the different mismatch between the Ba122:Co and the MgO or the STO, because the  $a$ -axis parameter of Ba122:Co ( $a = 0.396 \text{ nm}$ ) [14] is much closer to STO substrate ( $a = 0.39 \text{ nm}$ ), and therefore less strain develops in the Ba122:Co thin films compared with compressive strain in Ba122:Co thin films on MgO substrates ( $a = 0.42 \text{ nm}$ ).

Figure 2 shows the temperature dependence of the resistivity in different fields up to 9 T. The onset transition temperature  $T_c^{\text{onset}}$  and zero-resistance temperature  $T_c^{\text{zero}}$  of the Ba122:Co CCs are 20.2 and 19.0 K, respectively, where the  $T_c^{\text{onset}}$  is determined by the intersection of straight lines extrapolated from the normal state and the transition region, as shown by the green line in figure 2. The  $T_c$  of Ba122:Co thin films on STO layers is lower than similar thin films on IBAD-MgO metal tapes [9] or on CaF<sub>2</sub> single crystal substrates [15]. The reduction in  $T_c$  may be caused by strains in thin films, for it has been observed a linear dependence of  $T_c$  of Ba122:Co thin films on the epitaxial strain in the films [16]. As mentioned above, less strain has developed in the Ba122:Co thin films on STO layers, compared with MgO or CaF<sub>2</sub> substrates. Additionally, inhomogeneity in Ba122:Co thin films also adversely affects the superconducting properties [17, 18], while in the case of metal tapes inhomogeneity in

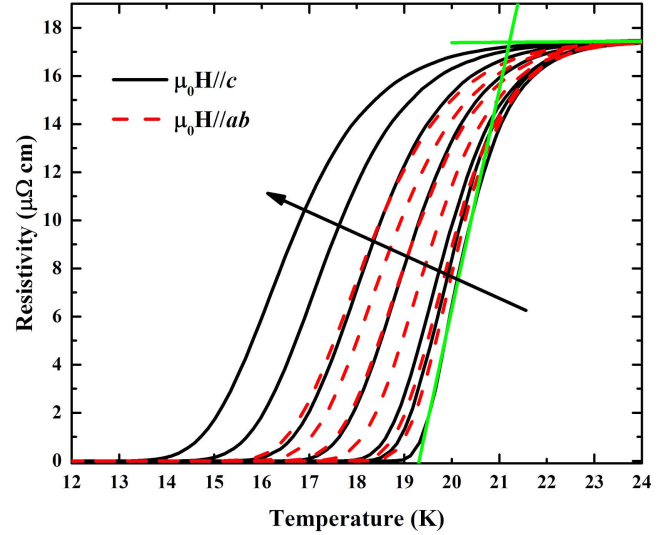


**Figure 2.** Temperature-dependent resistivity for Ba122:Co thin films in fields of 0, 0.4, 1, 3, 5, 7 and 9 T for  $H//ab$  and  $H//c$ . The green lines are extrapolated from the normal state and the transition region.

thin films will be induced due to the flexibility of metal tapes which may lead to an inhomogeneous surface temperature.

According to the Arrhenius dependence [19, 20], by virtue of the assumption  $U(T, H) = U_0(H)(1 - T/T_c)$ , we can get  $\ln\rho(T, H) = \ln\rho_0(H) - U_0(H)/T$  and  $\ln\rho_0(H) = \ln\rho_{0f} + U_0(H)/T_c$ , where  $U_0(H)$  is the activation energy for vortex motion and  $\rho_{0f}$  is a prefactor. Therefore, the activation energy  $U_0(H)$ , determined by the hopping of vortex bundles in the pinning potential, can be directly obtained from the slopes of the linear part of the Arrhenius plots of resistive transition in fields. Figures 3(a) and (b) show the Arrhenius plots of resistivity at various fields parallel to the  $c$ -axis and  $ab$ -plane, respectively. The slopes of the linear fit corresponding to  $U_0(H)$  in figures 3(a) and (b) are depicted in figure 3(c) as a function of field  $H$ . As can be seen in figure 3(c),  $U_0(H)$  exhibits a power law for the two main directions, i.e.,  $U_0(H) \propto \mu_0 H^{-\alpha}$ , with three distinct  $\alpha$  at different field regime. On the other hand, different field dependence of  $U_0(H)$  for different field region has also been observed in Ba122:Co and Ni-doped single crystal [21]. At low field regime ( $<1 \text{ T}$ ),  $U_0(H)$  drops very slowly, with field dependence as  $(\mu_0 H)^{-0.1}$  and  $(\mu_0 H)^{-0.04}$  for  $H//ab$  and  $H//c$ , respectively, implying an almost field-independent  $U_0$ , where single-vortex pinning dominates. The exponent  $\alpha$  at low field regime is similar to that observed in BaFe<sub>1.82</sub>Co<sub>0.18</sub>As<sub>2</sub> ( $\alpha = 0.09$ ) single crystal below 3 T [21], and similar small exponent  $\alpha$  was also observed in Ba<sub>0.72</sub>K<sub>0.28</sub>Fe<sub>2</sub>As<sub>2</sub> single crystal ( $\alpha = 0.09$  and 0.13 for  $H//ab$  and  $H//c$ , respectively) [22]. However, in the current case, as the field increases to mid-regime ( $\sim 1\text{--}3 \text{ T}$ ), the field dependence of  $U_0(H)$  falls into  $(\mu_0 H)^{-0.26}$  and  $(\mu_0 H)^{-0.34}$  for  $H//ab$  and  $H//c$ , respectively. Such exponents are different from single crystal case. At higher field ( $>3 \text{ T}$ ), a higher  $\alpha$  can be observed in the current case, with  $(\mu_0 H)^{-0.46}$  and  $(\mu_0 H)^{-0.89}$  for  $H//ab$  and  $H//c$ , respectively, where the higher value of the exponent  $\alpha$  in the high field indicates a collective flux creep regime. It is worth mentioning that the exponent  $\alpha$  for  $H//c$

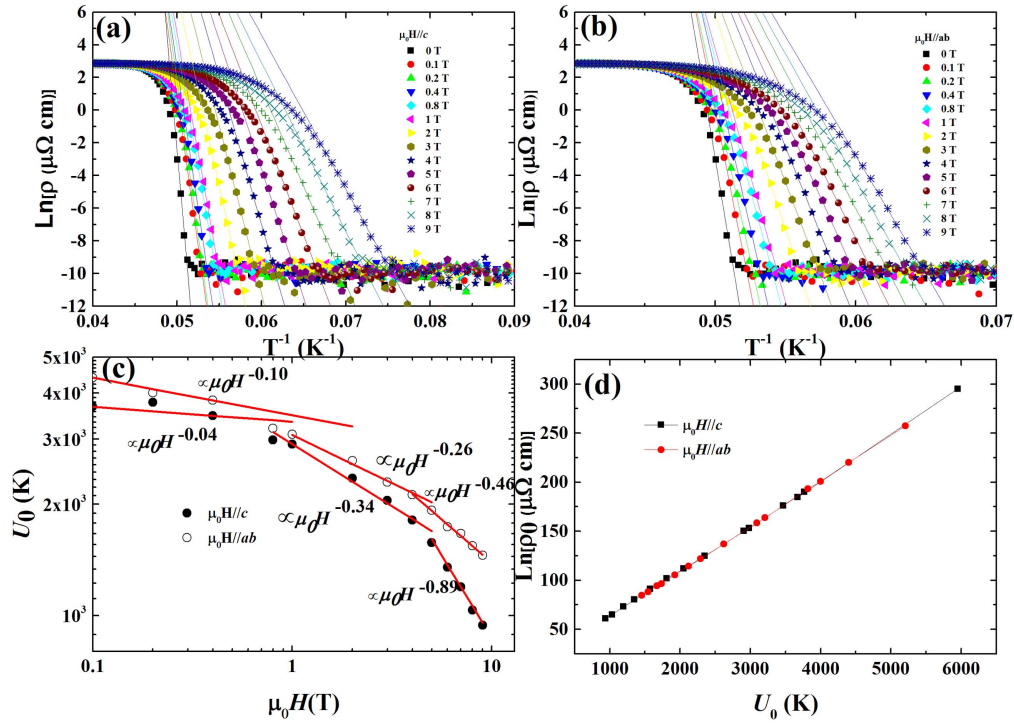


**Figure 3.** Arrhenius plots of the resistivity curves for  $H//c$  (a) and  $H//ab$  (b). The dotted lines in (a) and (b) represent the fitting results for the linear part in the Arrhenius plots. (c) Activation energy  $U_0$ (K) as a function of field determined from Arrhenius plots for  $H//ab$  and  $H//c$ . The red lines are the power law fitted for different field regions. (d)  $\ln\rho_0$  as a function of  $U_0$  for  $H//ab$  and  $H//c$ .

higher than 3 T is also similar to the those in  $\text{BaFe}_{1.82}\text{Co}_{0.18}\text{As}_2$  ( $\alpha = 0.9$ ) [21] and  $\text{BaFe}_{1.9}\text{Co}_{0.1}\text{As}_2$  ( $\alpha = 0.81$ ) [23] single crystals. The difference in exponent  $\alpha$  for intermediate fields ( $\sim 1$ –3 T) would suggest the coexistence of single-vortex pinning and collective flux creep at intermediate fields. In contrast to the above case of magnetic doping, in non-magnetic substitution, such as K doped Ba122 single crystal [22] or tapes by the PIT method [24],  $U_0(H)$  drops very slowly with field as  $(\mu_0 H)^{-0.09}$  and  $(\mu_0 H)^{-0.13}$  for  $H//ab$  and  $H//c$  throughout the entire field range, showing a field-independent exponent  $\alpha$  in the whole magnetic field range investigated. The different influence of different doping on pinning potential requires further study. Figure 3(d) shows the  $\ln\rho_0$  as a function of  $U_0$  for  $H//ab$  and  $H//c$ . One can see a clear linear behavior that can be fitted with  $\ln\rho_0(H) = \ln\rho_{0f} + U_0(H)/T_c$ . The linear fitting gives  $T_c$  of 21.6 K for both  $H//ab$  and  $H//c$ , close to the  $T_c$  determined from the  $R$ – $T$  curve. This perfect linear scaling also reveals the validity of the above assumption [25].

The transport current density  $J_c$  as a function of applied fields at 4.2, 6, 8, 10, 12 and 14 K for  $H//ab$  and  $H//c$  is given in figure 4. At 4.2 K, the  $J_c$  is  $1.14 \text{ MA cm}^{-2}$  in self-field and remains at 0.98 and  $0.86 \text{ MA cm}^{-2}$  up to 9 T for  $H//ab$  and  $H//c$ , respectively, showing better high field performance over other Ba122:Co CCs [8–10]. As shown in figure 4,  $J_c$  values for  $H//ab$  at each measurement temperature are always higher than those for  $H//c$ , indicating the flux pinning is anisotropic. At low temperatures, thin films show a slow decrease in  $J_c$  with fields. In order to obtain the vortex pinning information, we analyze the pinning force

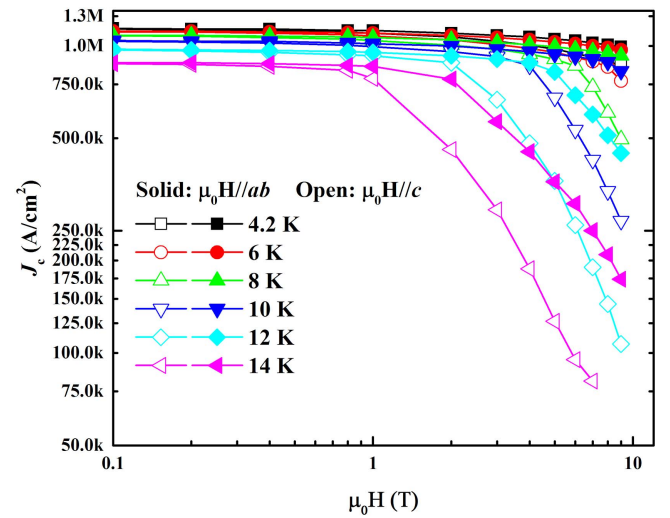


**Figure 4.** Transport current density  $J_c$  as a function of applied fields at different temperatures for  $\mu_0 H//ab$  and  $\mu_0 H//c$ .

$F_p = \mu_0 H \times J_c$ , as shown in figure 5. Figure 5(a) compares the  $F_p$  of Ba122:Co CCs at 12 K for  $H//ab$  and  $H//c$  with other CCs fabricated on IBAD-MgO metal tapes with [10] and without [9] Fe buffer layers, where significant enhancement of  $F_p$  can be observed, especially at high fields. It is worth noting that the  $F_p$  on Ba122:Co CCs are four and six times higher than that of CCs from IBAD-MgO with and without Fe buffer layers. In addition, the  $F_p$  is comparable to that of  $\text{Nb}_3\text{Sn}$  at 4.2 K [26] and much higher than that of NbTi



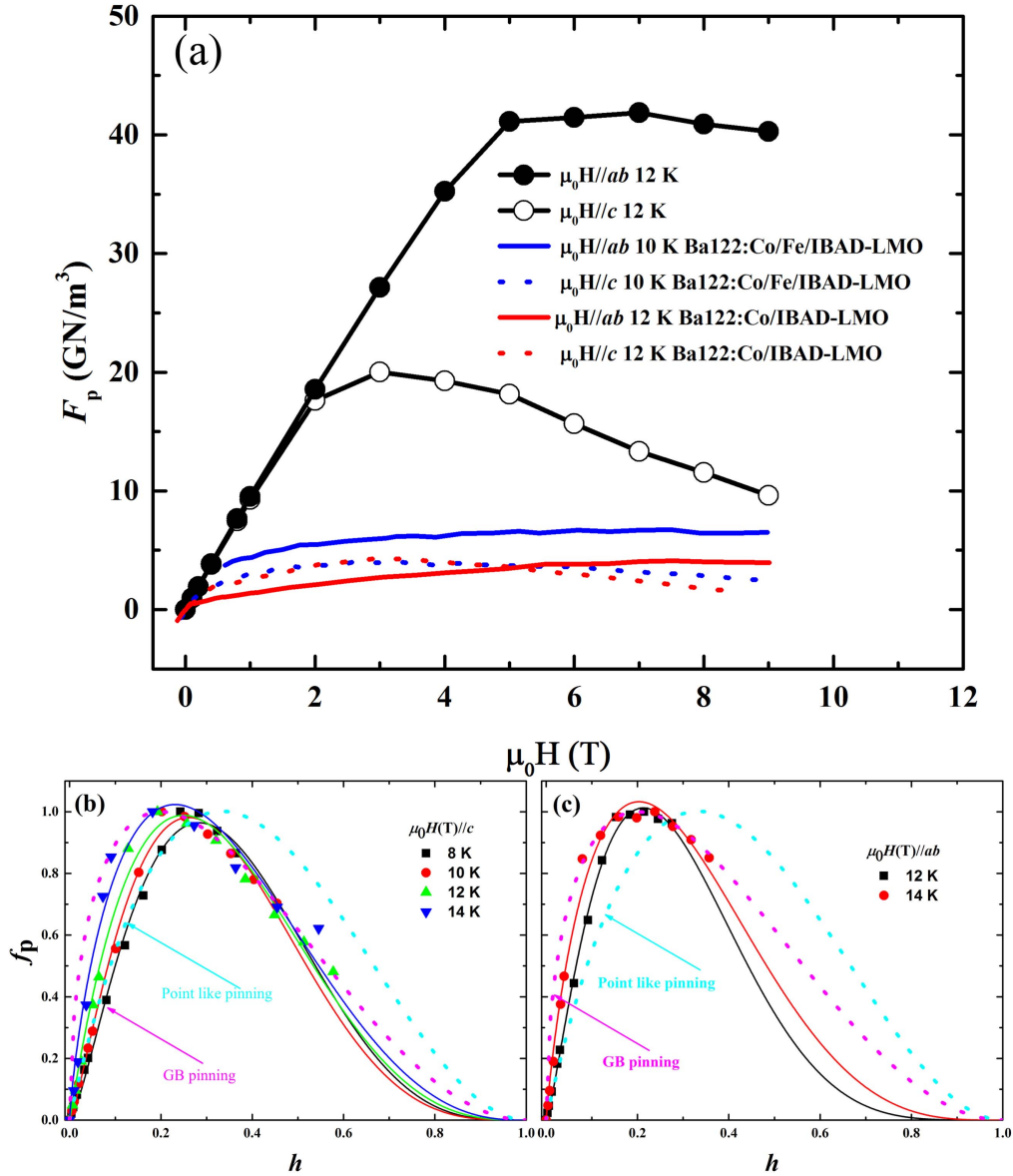


**Figure 5.** (a) Comparison of pinning force  $F_p$  for Ba122:Co CCs with Ba122:Co CCs from IBAD-LMO with [10] and without [9] Fe buffer layers for  $H // ab$  and  $H // c$ . The normalized pinning force  $f_p$  as a function of reduced field  $h$  for (b)  $H // c$  and (c)  $H // ab$ . The solid line is the fitting curve.

at 4.2 K [27]. Figures 5(b) and (c) compare the normalized pinning forces  $f_p = F_p / F_{p,max}$  as a function of the reduced magnetic field  $h = H / H_{irr}$  at different temperatures for  $H // ab$  and  $H // c$ , where  $H_{irr}$  is the irreversibility field determined by the Kramer extrapolation (not shown here). According to Kramer's scaling law approximation  $f_p \sim h^p (1 - h)^q$  [28], if only one pinning mechanism dominates at different temperatures, the normalized pinning force  $f_p$  would collapse into one single curve with similar  $p$  and  $q$  (8 K ( $p = 1.40$ ,  $q = 3.54$ ), 10 K ( $p = 1.28$ ,  $q = 3.61$ ), 12 K ( $p = 1.01$ ,  $q = 3.04$ ), 14 K ( $p = 0.80$ ,  $q = 2.67$ ) for  $H // c$ , and 12 K ( $p = 1.30$ ,  $q = 4.8$ ), 14 K ( $p = 0.88$ ,  $q = 3.43$ ) for  $H // ab$ ), implying a both field- and temperature-dependent

pinning mechanism. It can be observed that the parameter  $p$  decreases with increasing temperature for both major crystallographic directions of the applied field. According to the model proposed by Kramer [29] for shear breaking of the flux line lattice as the main reason for depinning and by Dew-Hughes [28] for pinning by planar defects such as grain boundary (GB) and twin boundaries, the fitting results would follow  $f_p \sim h^{0.5} (1 - h)^2$ . On the other hand, for a point-defect core pinning mechanism, the fitting result would follow  $f_p \sim h^1 (1 - h)^2$ . Dotted lines shown in figures 5(b) and (c) present the two cases. Therefore, the temperature-dependent  $p$  may indicate an evolution of the pinning mechanism.

To investigate the vortex pinning properties, angular dependence of  $J_c$  at different fields and temperatures was carried out, as shown in figure 6. At  $H // ab$  ( $\theta = 90^\circ$ ), an

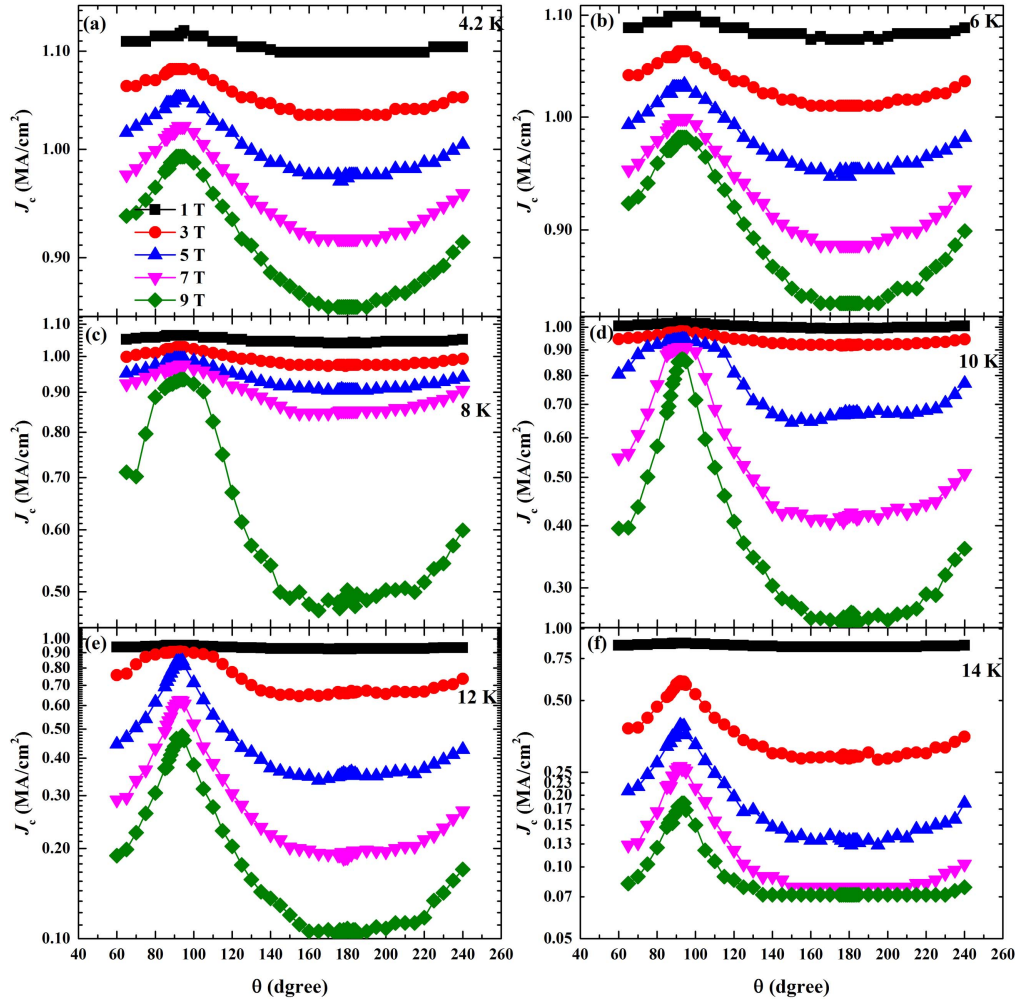


**Figure 6.** (a)–(f) Angular dependence of  $J_c$  for the Ba122:Co films at 4.2, 6, 8, 10, 12 and 14 K under fields of 1, 3, 5, 7 and 9 T.

obvious  $J_c$  peak was observed, mainly caused by the intrinsic pinning due to the correlated  $ab$ -planes arising from coupling between superconducting blocks, which are composed of metallic FeAs planes separated by spacer layers of alkaline earth. In addition, the  $J_c$  peak at  $H//ab$  becomes increasingly pronounced with increasing field. In contrast, no sign of  $J_c$  peaks except for a broad hump at  $H//c$  ( $\theta = 180^\circ$ ) above 8 K was observed in the whole temperature and field range. Such features of  $J_c$  for Ba122:Co thin films have been observed for those on single crystal substrates [30]. However, it also reported weak  $J_c$  peaks at  $H//c$  in Ba122 thin films [11, 15, 31, 32]. Such a divergence may be caused by the difference in deposition conditions, for example, it has been reported that the structural properties of the Ba122:Co thin films are very sensitive to the laser energy [33].

It has been demonstrated that anisotropic scaling approach proposed by Blatter [34] is quite a strong tool to identify the principle cause for the angular variation of  $J_c$ . Based on the approach, if pinning is only caused by random point defects,

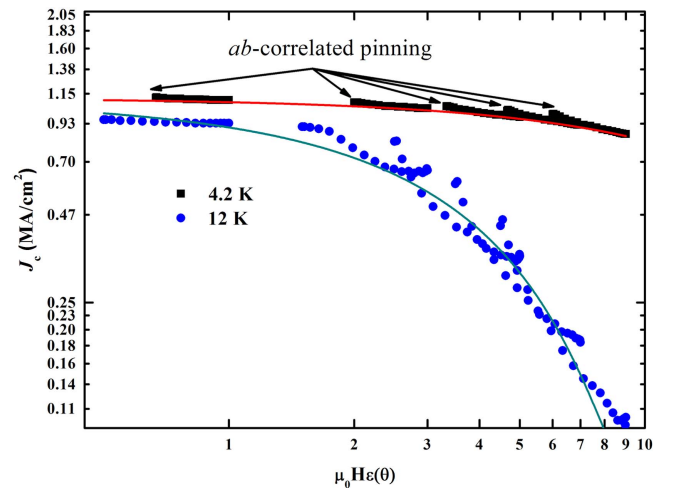


**Figure 7.** Scaling behavior of  $J_c(\theta)$  at 4.2 K and 12 K as a function of effective field. The solid lines are the fitting curve using the scaling function. The arrows indicate the locations related to the  $ab$ -correlated pinning.

i.e. uncorrelated disorder, the dependence of  $J_c$  on  $H$  and  $\theta$  can then be scaled with an effective field  $H_{\text{eff}} = \mu_0 H \varepsilon(\theta)$ ,  $J_c(H, \theta) = J_c(H_{\text{eff}})$ , where  $\varepsilon(\theta) = \sqrt{\cos^2(\theta) + \gamma^{-2} \sin^2(\theta)}$  and  $\gamma$  is the mass anisotropy, and the failure in scaling otherwise indicates the presence of other pinning mechanisms. The scaling behavior of  $J_c$  as a function of  $H_{\text{eff}}$  for two typical temperatures is given in figure 7. As shown in figure 7, the resulting curves for both 4.2 K and 12 K result cannot collapse onto a single curve with small anisotropies of  $\gamma = 1.5$  and 2 for 4.2 and 12 K [35], respectively. For the low temperature scaling behavior, all data excepted in the vicinity of  $H//ab$  collapse onto a single curve, indicating random point defects dominate in those regions. On the other hand, the deviations from the main trend close to the  $ab$ -plane with an angular range of  $\pm 20^\circ$  around  $90^\circ$  indicate the intrinsic pinning mechanism associated with the  $ab$ -correlated pinning. However, the scaling result at a higher temperature shows a behavior very different from that at a lower temperature, where data both in the vicinity of  $H//ab$  and  $H//c$  cannot collapse onto a single curve, implying that correlated defects also have some effect for  $H//c$  at a high temperature. This behavior may be a result of the broad hump at  $H//c$  and illustrates the complexity of the pinning in the Ba122:Co CCs. Compared with the low temperature results, a much stronger deviation from the main trend around  $H//ab$  can be observed at higher temperature, indicating the evolution of the pinning mechanism with temperature, which is in accordance with the result of normalized pinning force analysis.

As a link between conventional and cuprate superconductors, CCs based on IBSs are particularly attractive for large current and high field applications from low to medium temperatures. High-field-magnet applications are currently dominated by conventional superconductors, such as Nb<sub>3</sub>Sn and NbTi, but IBS CCs are a competing candidate due to their high  $H_{c2}$  and  $J_c$ . IBSs show great advantages in terms of production cost in comparison with cuprate superconductors. Compared with IBS thin films on single crystal substrates, CCs exhibit slightly lower superconducting properties, mainly caused by the low texture of the buffer layers. As discussed above, similar IBS thin films on metal tapes with different buffer layers, such as MgO, STO and Fe, present different transport properties, and therefore the role of buffer layers needs further attention.


In summary, we have investigated the transport properties on Ba122:Co thin films fabricated by PLD on metal tapes. The Ba122:Co thin films exhibit biaxially textured growth and high phase purity, confirmed by XRD. According to the transport measurement, a self-field  $J_c$  as high as  $1.14 \text{ MA cm}^{-2}$  and in-field  $J_c$  of 0.98 and  $0.86 \text{ MA cm}^{-2}$  up to 9 T have been achieved. The high transport  $J_c$ , especially at high field, makes this material promising for applications. The Ba122:Co CCs exhibit a significant enhancement in pinning force compared with similar Ba122:Co CCs from IBAD-MgO metal tapes. Activation energy  $U_0(H)$  determined by Arrhenius dependence shows a power law with three distinct exponents at a different field regime for both field orientations, indicating a transition from single-vortex pinning to

collective flux creep regime with field. A different pinning mechanism with field orientation can be seen from the angular dependence of  $J_c$ , where an obvious peak appears at  $H//ab$  with a less pronounced hump at  $H//c$  for high temperatures and fields. The anisotropic scaling approach reveals that intrinsic pinning associated with coupling between superconducting blocks determines the pinning in the vicinity of  $H//ab$ , whereas for  $H//c$  random point defects play a role at low field, but for high field correlated defects appear.

## Acknowledgments

The authors would like to express their thanks to Professor Dongning Zheng and Dr Hekang Li for help in the fabrication of micro bridges. This work is partially supported by the National Natural Science Foundation of China (Grant Nos. 51320105015, 51402292 and 51607174), the Beijing Municipal Science and Technology Commission (Grant No. Z171100002017006), the Bureau of Frontier Sciences and Education, Chinese Academy of Sciences (QYZDJ-SSW-JSC026), the Key Research Program of the Chinese Academy of Sciences (Grant No. XDPB01).

## ORCID iDs

Zhongtang Xu  <https://orcid.org/0000-0002-1812-3362>  
Yanwei Ma  <https://orcid.org/0000-0002-7131-0888>

## References

- [1] Chen X H, Wu T, Wu G, Liu R H, Chen H and Fang D F 2008 *Nature* **453** 761
- [2] Kamihara Y, Watanabe T, Hirano M and Hosono H 2008 *J. Am. Chem. Soc.* **130** 3296
- [3] Ren Z A et al 2008 *Chin. Phys. Lett.* **25** 2215
- [4] Tarantini C, Gurevich A, Jaroszynski J, Balakirev F, Bellingeri E, Pallecchi I, Ferdeghini C, Shen B, Wen H H and Larbalestier D C 2011 *Phys. Rev. B* **84** 184522
- [5] Yuan H Q, Singleton J, Balakirev F F, Baily S A, Chen G F, Luo J L and Wang N L 2009 *Nature* **457** 565
- [6] Katase T, Ishimaru Y, Tsukamoto A, Hiramatsu H, Kamiya T, Tanabe K and Hosono H 2011 *Nat. Commun.* **2** 409
- [7] Sato H, Hiramatsu H, Kamiya T and Hosono H 2016 *Sci. Rep.* **6** 36828
- [8] Iida K et al 2011 *Appl. Phys. Express* **4** 013103
- [9] Katase T, Hiramatsu H, Matias V, Sheehan C, Ishimaru Y, Kamiya T, Tanabe K and Hosono H 2011 *Appl. Phys. Lett.* **98** 242510
- [10] Trommler S, Hänisch J, Matias V, Hühne R, Reich E, Iida K, Haindl S, Schultz L and Holzapfel B 2012 *Supercond. Sci. Technol.* **25** 084019
- [11] Yuan P S, Xu Z T, Wang D L, Zhang M, Li J Q and Ma Y W 2017 *Supercond. Sci. Technol.* **30** 025001
- [12] Iida K, Sato H, Tarantini C, Hänisch J, Jaroszynski J, Hiramatsu H, Holzapfel B and Hosono H 2017 *Sci. Rep.* **7** 39951
- [13] Chen Y M et al 2008 *Mater. Res. Soc. Symp. Proc.* **1099** II01–I02

- [14] Ni N, Tillman M E, Yan J Q, Kracher A, Hannahs S T, Bud'ko S L and Canfield P C 2008 *Phys. Rev. B* **78** 214515
- [15] Tarantini C, Kametani F, Lee S, Jiang J, Weiss J D, Jaroszynski J, Hellstrom E E, Eom C B and Larbalestier D C 2014 *Sci. Rep.* **4** 7305
- [16] Lei Q Y *et al* 2014 *Supercond. Sci. Technol.* **27** 115010
- [17] Plecenik T, Gregor M, Sobota R, Truchly M, Satrapinskyy L, Kurth F, Holzapfel B, Iida K, Kus P and Plecenik A 2013 *Appl. Phys. Lett.* **103** 052601
- [18] Katase T, Hiramatsu H, Kamiya T and Hosono H 2010 *Appl. Phys. Express* **3** 063101
- [19] Palstra T T, Batlogg B, Schneemeyer L F and Waszczak J V 1988 *Phys. Rev. Lett.* **61** 1662
- [20] Jaroszynski J *et al* 2008 *Phys. Rev. B* **78** 174523
- [21] Ghorbani S R, Wang X L, Shabazi M, Dou S X, Choi K Y and Lin C T 2012 *Appl. Phys. Lett.* **100** 072603
- [22] Wang X L *et al* 2010 *Phys. Rev. B* **82** 024525
- [23] Shahbazi M, Wang X L, Ghorbani S R, Dou S X and Choi K Y 2012 *Appl. Phys. Lett.* **100** 102601
- [24] Zhang X P *et al* 2014 *Appl. Phys. Lett.* **104** 202601
- [25] Iida K *et al* 2013 *Sci. Rep.* **3** 2139
- [26] Godeke A 2006 *Supercond. Sci. Technol.* **19** R68
- [27] Cooley L D, Lee P J and Larbalestier D C 1996 *Phys. Rev. B* **53** 6638
- [28] Dew-Hughes D 2006 *Phil. Mag.* **30** 293
- [29] Kramer E J 1973 *J. Appl. Phys.* **44** 1360
- [30] Iida K, Hänisch J, Thersleff T, Kurth F, Kitzun M, Haindl S, Hühne R, Schultz L and Holzapfel B 2010 *Phys. Rev. B* **81** 100507 (R)
- [31] Tarantini C, Lee S, Kametani F, Jiang J, Weiss J D, Jaroszynski J, Folkman C M, Hellstrom E E, Eom C B and Larbalestier D C 2012 *Physical Review B* **86** 214504
- [32] Hänisch J *et al* 2015 *Sci. Rep.* **5** 17363
- [33] Hiramatsu H, Sato H, Katase T, Kamiya T and Hosono H 2014 *Appl. Phys. Lett.* **104** 172602
- [34] Blatter G, Feigel'man M V, Geshkenbein V B, Larkin A I and Vinokur V M 1994 *Rev. Mod. Phys.* **66** 1125
- [35] Kano M, Kohama Y, Graf D, Balakirev F, Sefat A S, McGuire M A, Sales B C, Mandrus D and Tozer S W 2009 *J. Phys. Soc. Jpn.* **78** 084719